Approximations To Camera Sensor Noise

Xiaodan Jin and Keigo Hirakawa

jinx01@udayton.edu, University of Dayton, Dayton, OH, 45469 USA
khirakawa1@udayton.edu, University of Dayton, Dayton, OH, 45469 USA

ABSTRACT

Noise is present in all image sensor data. Poisson distribution is said to model the stochastic nature of the photon arrival process, while it is common to approximate readout/thermal noise by additive white Gaussian noise (AWGN). Other sources of signal-dependent noise such as Fano and quantization also contribute to the overall noise profile. Question remains, however, about how best to model the combined sensor noise. Though additive Gaussian noise with signal-dependent noise variance (SD-AWGN) and Poisson corruption are two widely used models to approximate the actual sensor noise distribution, the justification given to these types of models are based on limited evidence. The goal of this paper is to provide a more comprehensive characterization of random noise. We concluded by presenting concrete evidence that Poisson model is a better approximation to real camera model than SD-AWGN. We suggest further modification to Poisson that may improve the noise model.

Keywords: Camera Sensor, Noise Approximation, Poisson.

1. INTRODUCTION

Rapid deployment of consumer and professional-grade digital cameras have spurred innovations in electronics in recent years. Yet, noise is present in all images captured by image sensors. Therefore, whether it be everyday snapshots or professional photography, noise is an inconvenient fact of digital photography that will continue to require our attention.

Image sensor noise is typically classified into the following categories: fixed pattern noise, banding noise, and random noise (this article focuses on the characterization of random noise). Although shot noise, thermal noise, saturation, and read noise are well-documented sources of random noise, other sources of signal-dependent noise such as Fano noise and quantization also contribute to the overall noise profile. We will briefly review various sources of noise (discussing stochastic models for each if known) in Section 2.

Appealing to the fact that variance of the sensor measurements typically scales linearly with the signal strength, two widely used models to approximate the sensor noise distribution are the additive Gaussian noise with signal-dependent noise variance (SD-AWGN) and Poisson corruption. The second order moment matching, however, does not capture the entire noise distribution (e.g. tail behavior) that is critical to the success of image denoising techniques. Section 3 takes aim at a more thorough comparisons of SD-AWGN and Poisson distributions (i.e. not just variance matching).

We repeat the assessment of approximated distributions in the wavelet transformed coefficients in Section 4. Under this scenario, we compare the wavelet noise to SD-AWGN as before, as well as to the Irwin and Skellam distributions—said to be the distribution of noise in Haar wavelet coefficients when the pixel domain signal suffers Poisson corruption.

2. BACKGROUND: SOURCES OF IMAGE SENSOR NOISE

Image sensor noise is generally classified into three categories. The so-called *fixed pattern noise* is a pixel-wise bias introduced to sensor measurements owing to manufacturing variabilities. Photoelectricity is typically read out in raster order by a bank of A/D converters operating in parallel, result of which is the *banding noise* caused by the per-line biases of the hardware. Fixed pattern and banding can be reduced by imposing strict manufacturing tolerance. Signal processing techniques to remove the fixed pattern and banding noise have been

proposed previously.[1–3] Because the noise is largely deterministic or repeatable, noise of these types behave predictably.

The third category of noise is the so-called *random noise*—sources include photon emission, photoelectric effects, dark current, thermal noise, etc. As described by quantum electrodynamics, specular reflection and refraction that occurs as a result of interactions between the light and matter is a form of electron-positron annihilation. The resultant distribution of photons emitted is referred to as *shot noise* and is classically modeled as Poisson.[4] As such, the variance of the number of photons accumulated during sensor integration scales linearly with the underlying light intensity (and the signal-to-noise power ratio is inversely proportional to the light intensity).

Light intensity measurements are made by recapturing photons (a process known as *photon transfer*), and photodiode is the most commonly found integrating detector for converting photons to current[4] (where the actual *pixel value* is a measurement of voltage across a capacitor that accumulates the charge). If each photon generates exactly one electron, then the photon transfer is known as a *pair production* and it is a deterministic process. Indeed, exactly one electron-hole pair is produced when the momentum of one photon is absorbed, and in this case the photocurrent scales exactly as the number of photons. However, some photon energy is used for breaking covalent bond and causing lattice vibration—a phenomenon known as *photoelectric effect*. This is stochastic photon transfer that also results in photocurrent, where the average number of electrons generated by photon arrival is proportional to the quantum efficiency.

Drawing on the work of Fano,[5] a canonical measure of the stochasticity of integrating detectors is a ratio κ of noise variance over signal strength ($\kappa = 0$ corresponds to the deterministic process of electron-hole pair production; on other hand, $\kappa = 1$ denotes Poisson distribution). The Fano factor for silicon (and by extension, Fano factor for CMOS sensor) is $\kappa = 0.12$, meaning that the photon transfer in a typical image sensor results in heteroskedastic noise.

Besides the noise associated with photon recapture via an integrating detector device, there are a number of sources for electrical noise on a typical sensor. The dark current stemming from in-circuit electron excitation and source follower results in *thermal noise*, whose power is proportional to the exposure time but is typically independent of the signal strength. *Reset noise* is the result of the improperly discharged capacitors, where measurement biases are introduced by the electrical charges previously held by the capacitors. Impreciseness caused by rounding and truncation during digitization of analog voltage is called *quantization error*, where the distribution of the difference between the actual analog signal value and quantized digital signal value is often approximated by additive white uniform distribution (though technically signal-dependent error).

Continuing hardware improvements have attenuated dark current and thermal noise significantly, and quantization error can be reduced with increased bitrate. However, photon emission and photoelectric effects are the foundations of the ways in which quantum mechanics enable image sensors that cannot be eliminated. Hence random noise is a "necessary evil" of image sensors that cannot be addressed by hardware improvements alone.

3. APPROXIMATION TO IMAGE SENSOR NOISE

3.1 Empirical Sensor Noise

We captured Macbeth ColorChecker using Nikon D90, Canon 5D Mark II, and Sony α57 in raw sensor format. They were captured under various ISO settings, and red, blue, and two green channels were separated (i.e. no demosaicking). Empirical mean and variance for each squares in the ColorChecker are calculated and shown in Figure 1. Assuming that fix pattern and banding noise are insignificant, this figure presents a convincing evidence that noise variance scales linearly with signal strength for the cameras considered. In the subsequent analysis, slope and intercept in Figure 1 were calculated using total least square fitting. From them, α and β noise parameters used in (1) and (3) below can be estimated (for the purpose of fitting model to the data). Automatic methods for determining α and β parameters have been proposed previously,[6–9] but this topic is outside the scope of this article.

The characteristics of red, green, and blue channels are very similar in Figure 1. This is consistent with the fact that the gain and timing registers on a typical color image sensor is set globally, and there are no major

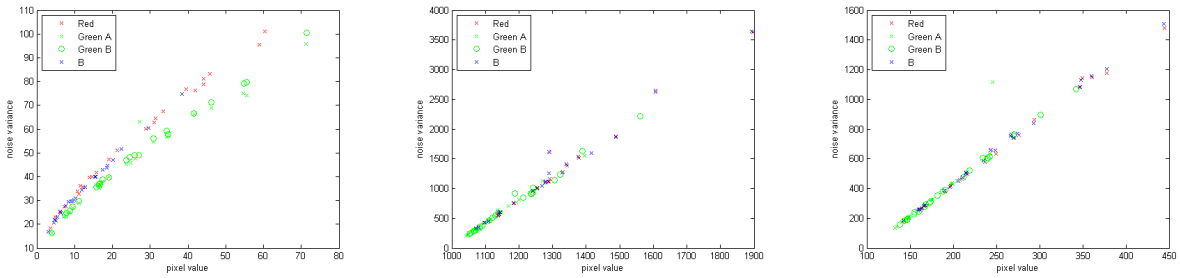

(a) Nikon D90 (b) Canon 5D Mark II (c) Sony α57

Figure 1. Measurements produced from a picture of Gretagmacbeth ColorChecker. The sample means of the pixel values observed within the same "squares" were plotted against the sample variances. (a) Raw sensor measurements acquired with Nikon D90 DSLR; (b) Raw sensor measurements acquired with Canon 5D Mark II DSLR; (c) Raw sensor measurements acquired with Sony α57 DSLR.

architectural differences in pixel sensors other than the absorptive color filters. As noise variance is strictly a function of the photon count and photon energy absorbed by the photodiode, the noise invariance to color filter is not surprising. On the other hand, a blue filter absorbs more light than green, limiting the number of photons that would reach the photodiode on a blue pixel. As proper white/color balancing is required, blue channel signal (and noise) is typically boosted more than green. Hence "post white balancing" noise variance in the blue channel significantly higher than green, a phenomenon that is widely reported.

3.2 SD-AWGN and Poisson Distributions

Let $\xi \sim \mathcal{N}(0,1)$. Then SD-AWGN model of an observation variable h takes the following form:

$$\begin{aligned} h &= \alpha g + \beta \\ g &= \pi f + \sqrt{\pi f}\xi \end{aligned} \tag{1}$$

where f is the true underlying light intensity and π is exposure. Here, the coupling between the signal and the noise variance arises by $\sqrt{\pi f}$ term, and the signal independent noise occurs as a result of β term (see below). The noise parameters α and β transform random variable g to yield an observation variable h whose variance is given by an affine relation

$$h|f \sim \mathcal{N}\big(\alpha\pi f + \beta, \alpha(\mathbb{E}\{h|f\} - \beta)\big). \tag{2}$$

It is worth noting that although this affine relation between the mean and variance of h is in agreement with Figure 1,[10] the Gaussianity of the distribution is often left unjustified in the literature.

For the Poisson distribution, pixel observation h' follows from the model:

$$\begin{aligned} h' &= \alpha g' + \beta \\ g' &\sim \mathcal{P}(\pi f), \end{aligned} \tag{3}$$

where α and β are the noise parameters relating Poisson variable g' and the observation h'. As before, the mean and the variance of the observations are in agreement with Figure 1:

$$\mathbb{E}\{h'|f\} = \alpha\pi f + \beta \tag{4}$$

$$\text{var}\{h'|f\} = \alpha(\mathbb{E}\{h'|f\} - \beta). \tag{5}$$

The fact that Poisson is a well accepted distribution for modeling photon emission suggests that the Poisson observation h' would match the actual sensor distribution better than the SD-AWGN observation h. Poisson on its own does not reflect other sources of sensor noise, such as Fano and dark current, however.

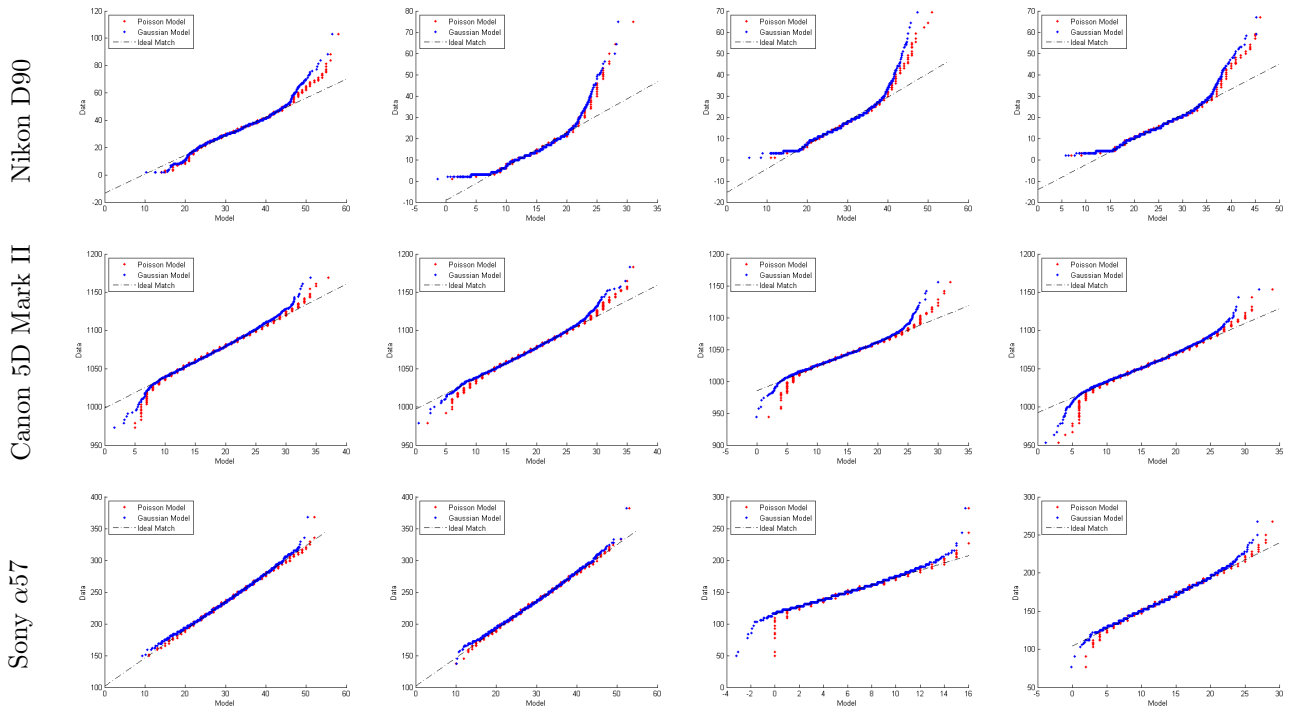

Figure 2. Q-Q plot comparing empirical sensor data to SD-AWGN and Poisson distribution models on red, blue and two green channels. Raw sensor measurements acquired with Nikon D90 DSLR, Canon 5D Mark II DSLR, and Sony α57 DSLR.

3.3 Quantile Analysis

Attributing the linearity in Figure 1 to the photon emission process, which is classically modeled as Poisson distributed, seems sensible at first glance. In practice, the photoelectric effects that is responsible for photon-to-electron conversion is also a source of heteroskedastic variabilities. Though SD-AWGN and Poisson are widely used to capture the heteroskedastic behavior,[6–9] the level of rigor employed to compare the noise models below extends beyond what was considered in the past.

Quartile analysis is a robust way to compare the distribution of data and model. Q-Q plot is defined by the parametric curve $(x(t), y(t))$ defined by

$$x(t) = F^{-1}_{\text{model}}(t), \qquad y(t) = F^{-1}_{\text{data}}(t),$$

where F_{data} and F_{model} are cumulative distribution functions of empirical data and model distributions, respectively, and $t \in [0, 1]$. Important feature of the Q-Q plot is that the curve lies on the 45° line if the empirical data and model distributions are identical; and is linear (but not 45°) if the data and the model variables are related by an affine transform (as in (1) and (3)). The differences in the data/model tails are visible if the curve strays from this line.

In the subsequent analysis, we first computed noise parameters α and β by fitting a line to Figure 1. Choosing a ColorChecker square (that is free of saturation), and then approximated the distribution of the pixels in this square by (1) and (3) using the ensemble mean $\mathbb{E}\{h|f\}$ as a parameter in addition to α and β. Q-Q plot comparing (1) and (3) to the empirical distribution of the pixels inside the ColorChecker square is shown in Figure 2. The model matches the sensor noise exactly if the plot lies exactly on the dotted line, which was calculated based on α and β.

Based on this analysis, Poisson and SD-AWGN have heavier positive tail and shorter negative tail than the empirical sensor data. As a general trend, Poisson's positive tail and SD-AWGN's negative tail are better

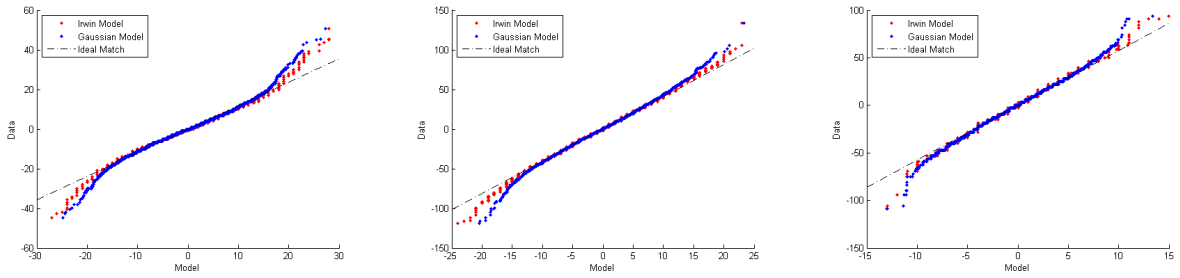

(a) Nikon D90 (b) Canon 5D Mark II (c) Sony α57

Figure 3. Q-Q plot comparing empirical wavelet data to SD-AWGN and Irwin distribution models on red, blue and two green channels. Raw sensor measurements acquired with Nikon D90 DSLR, Canon 5D Mark II DSLR, and Sony α57 DSLR.

matched with the empirical sensor data. Readers are cautioned that this graph does *not* imply that Poisson and SD-AWGN are better models for high and low intensity light, respectively. In fact, the larger/smaller sensor values represent positive and negative "noise" because each plot in Figure 2 assumes constant light intensity,

4. APPROXIMATION TO HAAR WAVELET NOISE

4.1 SD-AWGN and Skellam Distributions

Many image denoising methods are designed to operate in a (linear) transform domain. Among the popular transforms are wavelet and discrete cosine transforms. In order for these image denoising techniques succeed, it is important that the noise distribution is accurately modeled, especially the rate of tail decay and the degree of concentration near zero. To understand the effects that these transforms have on the noise models, we consider Haar wavelet transform. Haar wavelet transform is a convenient choice for this study because the effect it has on SD-AWGN and Poisson variables are well understood. Let h_i and h_i' be independent ith pixel SD-AWGN and Poisson variables in (1) and (3), respectively (g_i defined similarly, etc.). Then Haar coefficient models are:

$$w := h_1 - h_2 = \alpha(\underbrace{g_1 - g_2}_{s}), \qquad w' := h_1' - h_2' = \alpha(\underbrace{g_1' - g_2'}_{s'})$$

Under this scenario, we expect

$$s|f \sim \mathcal{N}\big(\pi f_1 - \pi f_2, \mathbb{E}\{h_1|f_1\} + \mathbb{E}\{h_2|f_2\} - 2\beta\big) \tag{6}$$

On the other hand, Haar transformed Poisson results is a Skellam distribution,[11,12] as follows:

$$s'|f \sim \mathit{Skellam}(\pi f_1 - \pi f_2, \mathbb{E}\{h_1|f_1\} + \mathbb{E}\{h_2|f_2\} - 2\beta). \tag{7}$$

In the special case that $f_1 = f_2$, the above distribution is called Irwin distribution.[13]

4.2 Quantile Analysis

We now repeat the quantile analysis for the Haar wavelet coefficients. Noise parameters α and β are computed as before. Because Q-Q plot requires sufficiently large number of samples, however, we cannot simply take the ensemble averages of pixel values in each ColorChecker square. Instead, we simulate the Haar coefficients in two ways. First, for the special case of $f_1 = f_2$, we randomly partition 50% of pixels in a chosen ColorChecker square and call them h_1; the remainder of the pixels are referred to as h_2. The empirical wavelet coefficients are generated from a randomized pair-wise subtraction $w = h_1 - h_2$, all of which are assumed to be drawn from the same distribution. These empirical wavelet coefficients are compared to SD-AWGN (6) and and Skellam (7) variables using Q-Q plots. Figure 3 shows representative Q-Q plot examples from each camera. As a general trend, Irwin and SD-AWGN models have shorter tails than the distribution of empirical wavelet coefficients.

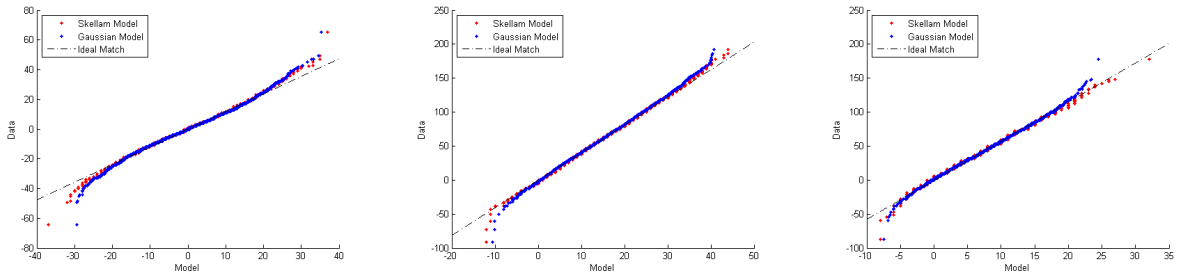

(a) Nikon D90 (b) Canon 5D Mark II (c) Sony α57

Figure 4. Q-Q plot comparing empirical wavelet data to SD-AWGN and Skellam distribution models on red, blue and two green channels. Raw sensor measurements acquired with Nikon D90 DSLR, Canon 5D Mark II DSLR, and Sony α57 DSLR.

Between the two models, however, Irwin's longer positive and negative tails clearly fit the data better than SD-AWGN.

Second, we simulate the scenario of $f_1 > f_2$ by choosing two ColorChecker squares. The empirical wavelet coefficients are generated by randomly sampling a pixel from each square and taking their differences. Again, the empirical wavelet coefficients can safely be assumed to be drawn from the same distribution, and they are compared to SD-AWGN and Skellam variables of (6) and (7) using Q-Q plots. The results in Figure 4 show that the positive tail of empirical wavelet coefficients is better represented by Skellam distribution than the SD-AWGN. The Skellam and SD-AWGN distribution fit the negative tail for Canon and Sony cameras better than the Nikon.

5. CONCLUSION

In this article, we discussed varioius sources of image sensor noise and provided a comprehensive characterization of random noise in image sensors. We compared the widely used SD-AWGN/Poisson/Irwin/Skellam distribution models to the distribution of the empirical sensor data using quantile analysis. Overall, the distribution of empirical sensor measurements has a longer tail than any models we considered. In the pixel domain, positive and negative tails were better approximated by Poisson and SD-AWGN, respectively. It suggests that a SD-AWGN-Poisson hybrid may improve the overall noise characterization. Irwin/Skellam were clearly better fit for the Haar wavelet coefficients than SD-AWGN. In practice, we expect Poisson-based image denoising methods to be better suited for processing real sensor data compared to the SD-AWGN-based ones. In fact, denoising methods that make use of even heavier noise tail is likely to improve performance for real sensor data. As future work, we will also consider combined AWGN-Poisson noise model.

ACKNOWLEDGMENTS

The authors would like to thank Bo Wen, Yi Zhang, Wu Cheng, Binu Nair, Temesguen Kebede and Dr. Vijay Asari of the University of Dayton for kindly assisting with sensor data collection.

REFERENCES

[1] G. Meynants, B. Dierickx, D. Uwaerts, and J. Bogaerts, "Fixed pattern noise suppression by a differential readout chain for a radiation-tolerant image sensor," in *IEEE Workshop on CCDs and AISs*, pp. 1–4, 2001.

[2] S. Cain, M. Hayat, and E. Armstrong, "Projection-based image registration in the presence of fixed-pattern noise," *IEEE Transactions on Image Processing* **10**(12), pp. 1860–1872, 2001.

[3] B. Zhang, J. Fadili, and J. Starck, "Wavelets, ridgelets, and curvelets for Poisson noise removal," *IEEE Transactions on Image Processing* **17**(7), pp. 1093–1108, 2008.

[4] J. Janesick, *Photon transfer*, SPIE-International Society for Optical Engineering, Washington, 2007.

[5] U. Fano, "Ionization yield of radiations. II. The fluctuations of the number of ions," *Physical Review* **72**(1), pp. 26–29, 1947.

[6] H. Talbot, H. Phelippeau, M. Akil, and S. Bara, "Efficient Poisson denoising for photography," in *Image Processing, 2009 16th IEEE International Conference on*, pp. 3881–3884, IEEE, 2009.

[7] A. Foi, M. Trimeche, V. Katkovnik, and K. Egiazarian, "Practical Poissonian-Gaussian noise modeling and fitting for single-image raw-data," *Image Processing, IEEE Transactions on* **17**(10), pp. 1737–1754, 2008.

[8] C. Liu, W. Freeman, R. Szeliski, and S. Kang, "Noise estimation from a single image," in *Computer Vision and Pattern Recognition, 2006 IEEE Computer Society Conference on*, **1**, pp. 901–908, IEEE, 2006.

[9] C. Liu, R. Szeliski, S. Kang, C. Zitnick, and W. Freeman, "Automatic estimation and removal of noise from a single image," *Pattern Analysis and Machine Intelligence, IEEE Transactions on* **30**(2), pp. 299–314, 2008.

[10] H. J. Trussell and R. Zhang, "The dominance of poisson noise in color digital cameras," in *IEEE International Conference on Image Processing (ICIP-2012)*, IEEE, 2012.

[11] J. Skellam, "The frequency distribution of the difference between two poisson variates belonging to different populations.," *Journal of the Royal Statistical Society. Series A (General)* **109**(Pt 3), p. 296, 1946.

[12] K. Hirakawa and P. Wolfe, "Skellam shrinkage: Wavelet-based intensity estimation for inhomogeneous poisson data," *Information Theory, IEEE Transactions on* **58**(2), pp. 1080–1093, 2012.

[13] J. Irwin, "The frequency distribution of the difference between two independent variates following the same poisson distribution," *Journal of the Royal Statistical Society* , pp. 415–416, 1937.